RESEARCH ARTICLE

Alkenyl oxindole is a novel PROTAC moiety that recruits the CRL4^{DCAF11} E3 ubiquitin ligase complex for targeted protein degradation

Ying Wang[1☯], Tianzi Wei[2☯], Man Zhao[1☯], Aima Huang[3], Fan Sun[3], Lu Chen[1], Risheng Lin[2], Yubao Xie[1], Ming Zhang[1], Shiyu Xu[3], Zhihui Sun[3], Liang Hong[3]*, Rui Wang[1,4]*, Ruilin Tian[2]*, Guofeng Li[1]*

1 School of Pharmacy, Shenzhen University Medical School, Shenzhen University, Shenzhen, China, 2 Key University Laboratory of Metabolism and Health of Guangdong, Department of Medical Neuroscience, School of Medicine, Southern University of Science and Technology, Shenzhen, China, 3 Guangdong Key Laboratory of Chiral Molecule and Drug Discovery, School of Pharmaceutical Sciences, Sun Yat-sen University, Guangzhou, China, 4 Institute of Materia Medica and Research Unit of Peptide Science, Chinese Academy of Medical Sciences and Peking Union Medical College, Beijing, China

☯ These authors contributed equally to this work.
* hongliang@sysu.edu.cn (LH); wangrui@lzu.edu.cn (RW); tianrl@sustech.edu.cn (RT); liguofeng@szu.edu.cn (GL)

Abstract

Alkenyl oxindoles have been characterized as autophagosome-tethering compounds (ATTECs), which can target mutant huntingtin protein (mHTT) for lysosomal degradation. In order to expand the application of alkenyl oxindoles for targeted protein degradation, we designed and synthesized a series of heterobifunctional compounds by conjugating different alkenyl oxindoles with bromodomain-containing protein 4 (BRD4) inhibitor JQ1. Through structure-activity relationship study, we successfully developed JQ1-alkenyl oxindole conjugates that potently degrade BRD4. Unexpectedly, we found that these molecules degrade BRD4 through the ubiquitin-proteasome system, rather than the autophagy-lysosomal pathway. Using pooled CRISPR interference (CRISPRi) screening, we revealed that JQ1-alkenyl oxindole conjugates recruit the E3 ubiquitin ligase complex CRL4^{DCAF11} for substrate degradation. Furthermore, we validated the most potent heterobifunctional molecule HL435 as a promising drug-like lead compound to exert antitumor activity both in vitro and in a mouse xenograft tumor model. Our research provides new employable proteolysis targeting chimera (PROTAC) moieties for targeted protein degradation, providing new possibilities for drug discovery.

Introduction

Targeted protein degradation (TPD) has emerged as a promising approach for drug discovery. It uses multispecific small molecules to selectively recognize target proteins, facilitating their degradation via cell's intrinsic protein degradation pathways [1]. Compared with traditional inhibitors, TPD drugs possess the unique ability to not only inhibit protein activity but also

facilitate the degradation of target proteins. This dual functionality empowers TPD drugs to elicit stronger therapeutic effects and holds promise for targeting proteins that were previously deemed "undruggable" [2–4]. Currently, TPD strategies primarily utilize 2 major degradation pathways: the ubiquitin-proteasome system and the lysosomal degradation pathway [5–7]. According to mechanism of action, the major TPD strategies include proteolysis targeting chimeras (PROTACs), lysosome targeting chimeras (LYTACs), and autophagy targeting chimeras (AUTACs) [8–11]. Among them, PROTAC technology is the most extensively studied and has achieved significant breakthroughs. It has been successfully applied to degrade more than 100 target proteins, including those previously considered "undruggable" [12]. Moreover, more than 20 PROTACs are currently undergoing clinical trials since 2019 [13–16], indicating that PROTAC technology is a promising strategy for drug discovery.

PROTACs are heterobifunctional molecules consisting of 2 ligand domains joined by a chemical linker. One ligand domain binds to the protein target of interest, and the other ligand recruits an E3 ubiquitin ligase. By engaging with both the target protein and E3 ligase simultaneously, PROTACs facilitate the polyubiquitination and proteasomal degradation of the target protein [17]. While over 600 E3 ligases have been identified in the human genome [18], only a small fraction (<3%) have been successfully recruited by PROTACs [19]. The most commonly utilized E3 ligases include CRBN, VHL, MDM2, and IAPs. More recently, KEAP1 [20,21], RNF114 [22,23], DCAF15 [24], and DCAF16 [25] have expanded the toolbox of accessible E3 ligases. However, the vast majority (>90%) of reported PROTAC molecules continue to rely on just 2 ligases: CRBN and VHL [12]. This narrow E3 diversity poses a major challenge, as the development and targeting potential of PROTAC degraders is constrained by the limited pool of recruited E3s. Therefore, broadening the range of E3 ligases that can be engaged by small molecule ligands could unlock new avenues to potentially degrade a wider range of protein targets, as well as circumvent the acquired drug resistance that caused by mutations in certain E3 ligases [26,27].

The alkenyl oxindole framework is commonly found in synthetic or natural compounds that exhibit a wide range of biological activities and have attracted research interests from pharmacologists and chemists [28]. Many alkenyl oxindoles have been developed as lead compounds or marketed drugs against tumors, such as sunitinib [29–31]. Recently, 2 alkenyl oxindoles (**10O5** and **AN1**) were found to act as molecular glues that tether mutant huntingtin protein (mHTT) to autophagy-related protein LC3, leading to the autophagy-lysosomal degradation of mHTT [32]. This prompted us to test whether this strategy can be expanded to degrade other substrates. To this end, we synthesized a series of heterobifunctional molecules by linking BRD4 inhibitor JQ1 with different alkenyl oxindoles, followed by assessing their targeted degradation activity. This led to the identification of HL435, a highly potent alkenyl oxindole-based BRD4 degrader. However, when we investigated the protein degradation mechanism of HL435, we found that it degraded BRD4 through the ubiquitin-proteasome system rather than the autophagy-lysosomal pathway. Based on this unexpected finding, we hypothesized that alkenyl oxindoles may act as novel E3 ligase ligands. To verify our hypothesis, we performed a pooled CRISPR interference (CRISPRi) screening, from which we revealed that the E3 ligase complex CRL4^{DCAF11} is in charge of HL435-induced proteasomal degradation of BRD4. We further validated the antitumor efficacy of HL435 both in vitro and in vivo. Overall, we discovered that alkenyl oxindoles can act as recruitment moiety for CRL4^{DCAF11} and developed alkenyl oxindole-based PROTAC molecules with high degradation efficiency and antitumor effects, expanding the toolbox of E3 ligases available for PROTAC drug development.

Results

Compounds development and structure-activity relationship studies on alkenyl oxindole-based heterobifunctional degraders
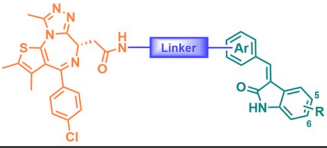
To explore the potential of alkenyl oxindole for target protein degradation, we designed and synthesized a series of heterobifunctional molecules by connecting JQ1 with different alkenyl oxindoles using various linkers (S1 Data), followed by examining their ability to degrade BRD4 (Figs 1 and S1). Firstly, JQ1 and the reported alkenyl oxindole (**10O5**) were connected directly with saturated or unsaturated alkane chains of different lengths to afford compounds **H1**-**H4**. However, they had little ability to degrade BRD4. When PEG linker was used to replace the alkane chain (**H5**), the degradation of BRD4 was observed at a concentration of 1.0 μM. Furthermore, the direct connection of linker and **10O5** through amide bond (**H6**) significantly improved the degradation ability. Therefore, we conducted a subsequent structural-activity study on the alkenyl oxindole moiety using the linker of compound **H6**. Subsequently, we examined the degradation activity of JQ1-alkenyl oxindole conjugates constructed from different alkenyl oxindole derivatives, including the addition of electron-poor substituents on the phenyl group or the benzo moiety of oxindole core (Fig 1 and **H7**-**H28**). The results showed that enhanced degradation activity can be achieved by substituting the alkenyl oxindole with trifluoromethyl group (Fig 1, R = 6-CF_3). These modifications led to the development of HL435 (**H27**), an excellent BRD4 degrader with a degradation efficiency >99% at 1.0 μM.

The NMR Spectra showed that there are (*E*) and (*Z*) isomers in all JQ1-alkenyl oxindole conjugates we synthesized. In order to clarify whether the isomeric configuration affects its efficacy in degrading BRD4, we separated and purified the 2 isomeric forms of compound **H6** through high-performance liquid chromatography (HPLC), and the western blot (WB) results demonstrated that there was no notable disparity in BRD4 degradation activity between the 2 configurations (S2 Fig). We subsequently explored the stability of the isomeric configuration and found that both configurations in methanol would undergo isomerization over time at different temperatures, with the isomerization rate noticeably decelerated at lower temperatures (S3 Data). This observation might partially account for the absence of significant differences in degradation activity between the isomeric configurations.

HL435 potently degrades BRD4 through the ubiquitin-proteasome system

To evaluate the efficacy of HL435 (Fig 2A) in depleting BRD4, we conducted a concentration-dependent study in human breast cancer cell lines (Figs 2B and S3A). The maximum degradation efficiency (D_{max}) of HL435 was >99%, with DC_{50} values of 11.9 and 21.9 nM in MDA-MB-231 and MCF-7 cells, respectively (Fig 2C). Kinetics study of BRD4 degradation showed that degradation was observed just 1 hour after HL435 treatment (Figs 2D and S3B), with a half-life of 1.38 and 1.31 hour in MDA-MB-231 and MCF-7 cells (Fig 2E), respectively. Meanwhile, HL435 was demonstrated to efficiently degrade BRD4 in a concentration-dependent manner in multiple cell lines (S4 Fig). Although the efficacies varied slightly among different cell lines, the D_{max} all >95%.

To validate the mechanism of BRD4 depletion induced by HL435, we first assessed the mRNA level of *BRD4*. The mRNA level of *BRD4* in the HL435-treated group was not lower than that of control group in breast cancer cells, indicating that HL435 did not affect BRD4 at the transcriptional level but rather at the protein level (Fig 2F). Alkenyl oxindoles were found to bind both LC3 and mHTT for inducing autophagy degradation of mHTT [32], so we explored whether autophagy-lysosomal inhibitors could rescue the degradation of BRD4 induced by JQ1-alkenyl oxindole-conjugated compounds. Surprisingly, both CQ and

Compound	Linker		Alkenyl Oxindole	BRD4 Degradation Rate (%)[a]	
				0.1 µM	1.0 µM
H1			R = 5-I	<10	10
H2			R = 5-I	<10	<10
H3			R = H	<10	<10
H4[b]			R = H	12	10
H5			R = H	<10	38
H6			R = H	25	49
H7			R = 5-I	22	50
H8			R = 5-F	35	86
H9			R = 5-Cl	44	78
H10			R = 5-Br	30	71
H11			R = 6-CF$_3$	52	96
H12			R = 5-F	-	24
H13			R = 5-Cl	-	30
H14			R = 5-Br	-	30
H15			R = 6-CF$_3$	-	55
H16			R = 5-F	-	47
H17			R = 5-Cl	-	38
H18			R = 5-Br	<10	34
H19			R = 6-CF$_3$	<10	59
H20			R = 5-F	12	62
H21			R = 5-Cl	28	32
H22			R = 5-Br	<10	55
H23			R = 6-CF$_3$	35	88
H24			R = 5-F	28	89
H25			R = 5-Cl	52	94
H26			R = 5-Br	53	95
H27 (HL435)			R = 6-CF$_3$	87	>99
H28			R = 6-CF$_3$	27	60

Fig 1. The structure and target degradation activity of JQ1-alkenyl oxindole conjugates. [a]BRD4 degradation rate was relative quantification result of S1 Fig (WB). [b]The Ar motif of H4 was 4-iodobenzaldehyde.

https://doi.org/10.1371/journal.pbio.3002550.g001

bafilomycin failed to rescue the degradation of BRD4 induced by HL435, **H1**, **H6,** or **H7** in different cell lines (Figs 2G, 2H, S5B and S5D). We next treated WT-, *ATG5KO*-, and *ATG4BKO*-Hela cells with HL435 and found that the absence of LC3 or autophagosomes did not affect the efficiency of HL435 in degrading BRD4 (Fig 2I). Similar results were obtained for **H1** (S5C Fig). These results suggested that the degradation of BRD4 by JQ1-alkenyl oxindole-conjugated compounds was independent of the autophagy-lysosomal pathway; thus, we suspected
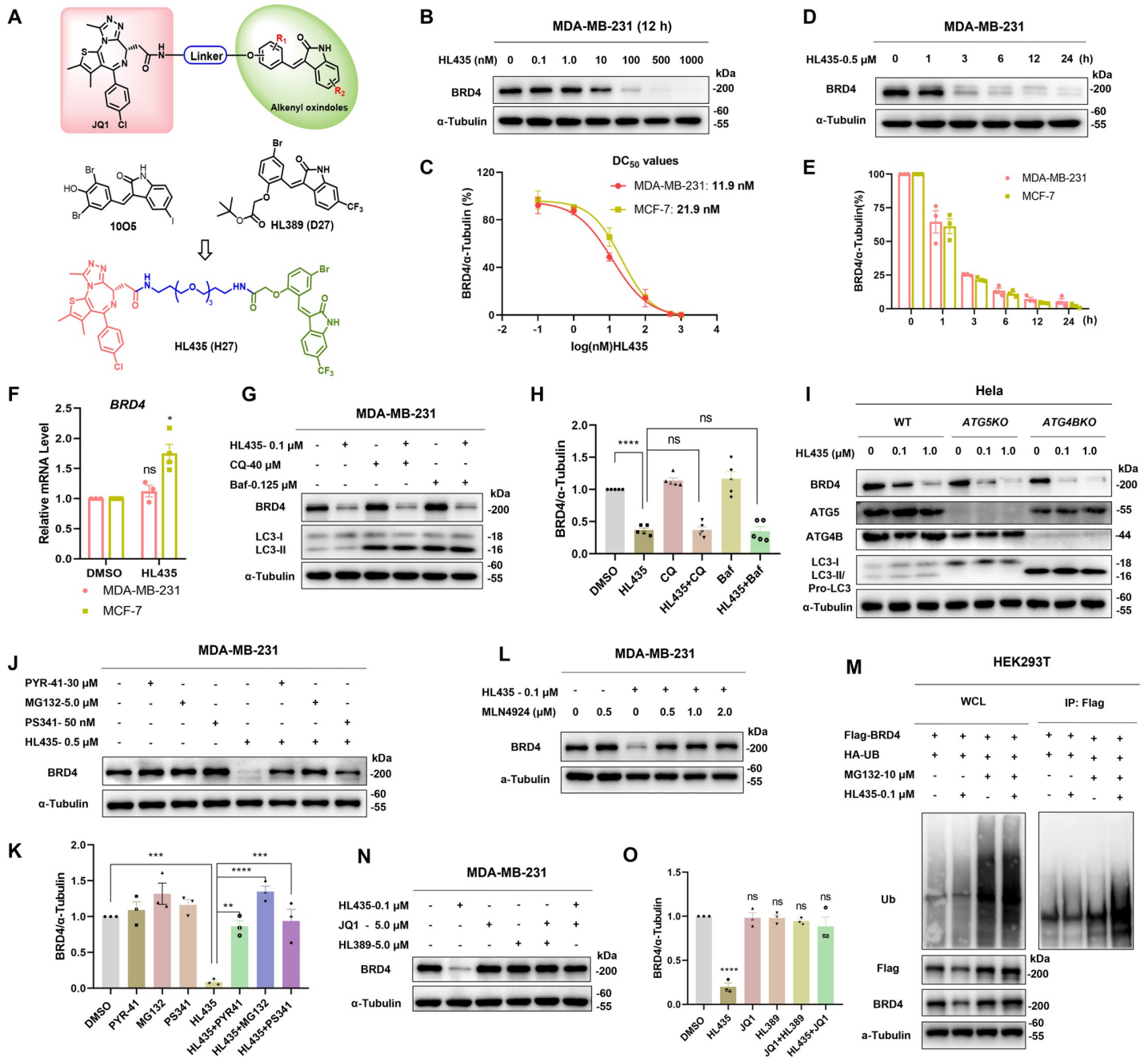
Fig 2. HL435 potently degrades BRD4 through the ubiquitin–proteasome system. (**A**) Design and development of HL435 as a potent BRD4 degrader. (**B**) Representative WB results; cells were treated with gradient concentrations of HL435 for 12 hours. (**C**) The DC_{50} values of HL435 to degrade BRD4 in MDA-MB-231 and MCF-7 cells, from relative quantitative analysis. (**D**) Representative WB results; MDA-MB-231cells were treated with HL435 at 0.5 μM for gradient time. (**E**) Relative quantitative analysis for the time-dependent degradation of BRD4. (**F**) The relative mRNA levels of *BRD4*; cells were treated with HL435 at 1.0 μM for 12 hours, GAPDH used as internal reference. (**G**) Representative WB results; cells were cotreated with HL435 and chloroquine (CQ) or bafilomycin (Baf) for 6 hours; CQ or Baf was pretreated for 2 hours. (**H**) Relative quantitative analysis of BRD4 from **G**. (**I**) Representative WB results (*n* = 3). *WT*-Hela, *ATG5KO*-Hela, or *ATG4BKO*-Hela cells were treated with indicated concentration of HL435 for 6 hours. (**J**) WB results for BRD4 degradation; cells were pretreated with PYR-41, MG132, or PS-341 for 2 hours, followed by HL435 cotreatment for 6 hours. (**K**) Relative quantitative analysis of BRD4 from **J**. (**L**) WB results; HL435 and MLN4924 were cotreated at indicated concentration for 6 hours; MLN4924 was pretreated for 2 hours. (**M**) Representative WB results. HEK293T cells were cotransfected with Flag-BRD4 and HA-Ub plasmids for 32 hours, followed by treatment with MG132 for 8 hours and HL435 for 6 hours. Cell lysates were immunoprecipitated with anti-Flag magnetic beads and immunoblotted for ubiquitination level of BRD4. (**N**) Representative WB results; JQ1, HL389, or HL435 was treated for 6 hours. (**O**) Relative quantitative analysis BRD4 from **N**. The data underlying the graphs in the figure can be found in S5 Data; the raw images for WB in the figure can be found in S1 Raw Images. Data were presented as mean ± SEM. Statistical significance was determined by one-way analysis of variance (ANOVA) or Mann–Whitney test (for **F**). *$p < 0.05$, **$P < 0.01$, ***$P < 0.001$, ****$P < 0.0001$; ns, no statistical significance.

https://doi.org/10.1371/journal.pbio.3002550.g002

that it was perhaps mediated by ubiquitin-proteasome system. To validate this hypothesis, E1 ubiquitin-activating enzyme inhibitor PYR-41 or proteasome inhibitors MG132 or PS-341 was employed to cotreatment with our compounds. As expected, pretreatment with PYR-41, MG132, and PS-341 all successfully rescued the degradation of BRD4 induced by HL435, **H6,** or **H7** (Figs 2J, 2K, S5D and S5E). Pretreatment with NEDD8 activating E1 enzyme (NAE1) inhibitor MLN4924 also block the degradation of BRD4 by HL435 (Fig 2L), indicating that the degradation required the activation of Cullin-RING E3 ligase (CRL). When the degradation process was blocked by proteasome inhibitor MG132, HL435 increased the ubiquitination level of BRD4 (Fig 2M). Finally, we validated that both JQ1 and structurally modified alkenyl oxindole HL389, whether used alone or in combination, cannot deplete BRD4 in MDA-MB-231 cells. Moreover, an excess of JQ1 could competitively block the degradation of BRD4 induced by HL435 (Fig 2N and 2O). All these results suggested that JQ1-alkenyl oxindole-conjugated compounds including HL435 degrade BRD4 through the ubiquitin-proteasome system rather than the autophagy-lysosomal pathway, and the degradation process depends on compounds simultaneously interacting with the substrate protein and the ubiquitin-proteasome system.

A focused CRISPRi screening identified CRL4^{DCAF11} complex potentially responsible for HL435-induced proteasomal degradation activity

To identify the E3 ligase mediating HL435-induced degradation of BRD4, we determined to conduct a pooled CRISPRi screening. We first constructed a dual-fluorescence reporter, containing the BRD4 bromodomain 1 (BD1) fused to mScarlet, followed by a P2A self-cleaving fragment and an enhanced green fluorescent protein (EGFP) for normalization (Fig 3A). This reporter was stably transduced into HEK293T cells constitutively expressing the CRISPRi machinery (dCas9-BFP-KRAB) from the CLYBL safe harbor locus [33]. Upon treatment with HL435, the relative BD1 intensity was significantly reduced, which could be fully prevented by MG132 (Fig 3B–3D), confirming the sensitivity of the reporter. Next, we designed a focused sgRNA library targeting all known human E1, E2, and E3 enzymes, consisting of 5,071 sgRNAs against 993 genes with 5 sgRNAs per gene, and more than 100 nontargeting control sgRNAs. Using this library, we performed a fluorescence activated cell sorting (FACS)-based CRISPRi screening in the BD1 reporter cells based on relative BD1-mScarlet signal (BD1-mScarlet intensity normalized to EGFP intensity). In the HL435-treated group, knockdown of any components mediating HL435-induced degradation activity would result in an increased relative BD1-mScarlet signal (Fig 3E), which would not increase in the DMSO-treated group. As shown in Fig 3F and 3H, components of the CRL4^{DCAF11} complex, including the E3 ligase scaffold Cullin-4B (*CUL4B*), the RING-finger protein RING-box1 (*RBX1*), the adaptor Damage-specific DNA binding protein 1 (*DDB1*), and the substrate receptor DDB1 and CUL4 associated factor 11 (*DCAF11*), were among the top positive hits, whose knockdown increased BD1-mScarlet signal in the HL435-treated group. In addition, *NAE1* and ubiquitin like modifier activating enzyme 3 (*UBA3*), which are responsible for CRL neddylation and activation, were also strong hits in the screening (Fig 3F). Importantly, these genes showed no phenotype or only weak phenotype in the DMSO group. These data indicated that the CRL4^{DCAF11} complex is specifically involved in HL435-induced substrate degradation (Fig 3F and 3G and S4 Data).

To validate the requirement of CRL4^{DCAF11} complex for the degradation activity of HL435, we individually cloned 2 separate sgRNAs targeting each of the following genes: *DCAF11*, *DDB1, CUL4B, RBX1, NAE1*, and *UBA3*, followed by evaluating their effects on HL435-induced BD1 reporter degradation (Fig 4A). As expected, knocking down any of these genes blocked the BD1 reporter degradation upon HL435 treatment (Fig 4B–4D). Additionally, we
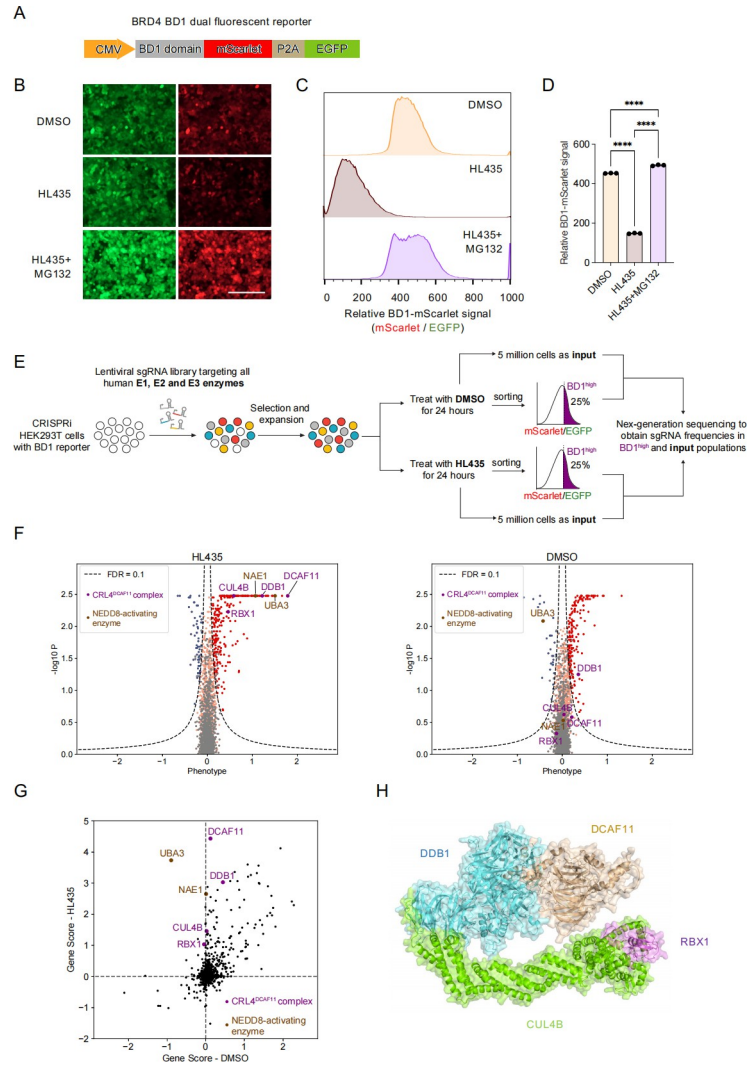
Fig 3. CRISPRi screening identified the CRL4^{DCAF11} complex as a potential target mediating HL435-induced proteasomal degradation of BRD4. (**A**) Design of BRD4 BD1 dual fluorescent reporter. BRD4 BD1 domain was fused with mScarlet, followed by a P2A self-cleaving fragment and an EGFP. (**B**) Validation of BD1 reporter response to HL435 treatment. Representative fluorescent microscope fields for BD1 reporter levels in HEK29T cells treated with DMSO, HL435 (50 nM), or HL435 (50 nM) and MG132 (5 μM) for 24 hours. Bar = 200 μm. (**C**) Validation of BD1 reporter response to HL435 treatment. Relative BD1-mScarlet signal in HEK293T cells was determined by the ratio of mScarlet and EGFP as measured by flow cytometry. The cells were treated with DMSO, HL435 (50 nM), or HL435 (50 nM) and MG132 (5 μM) for 24 hours. (**D**) Quantification of the relative BD1-mScarlet signal in the indicated groups was shown in the bar graph (mean ± SD, n = 3 biological replicates). The data underlying this graph can be found in S5 Data. (**E**) CRISPRi screening strategy. CRISPRi HEK293T cells harboring BD1 reporter were transduced with an sgRNA library targeting all human E1, E2, and E3 enzymes. Cells were treated with DMSO or HL435 (50 nM, 24 hours) and 5 million cells were taken as "input." Cells with top 25% relative BD1-mScarlet signal (BD1^{high}) were sorted via FACS. The frequencies of BD1^{high} and input cells expressing each sgRNA were determined by next-generation sequencing and were compared to determine sgRNAs enriched or depleted in the BD1^{high} population. The screening was performed in duplicates. (**F**) Screening results analyzed by the MAGeCK-iNC pipeline were shown for HL435-treated and DMSO-treated groups. A positive phenotype indicates the corresponding sgRNA was enriched in the BD1^{high} population and vice versa. Dots in red, blue, grey, and orange represent positive hits, negative hits, negative control, and other genes, respectively. Genes encoding components of the CRL4^{DCAF11} complex and the NEDD8-activating enzyme were highlighted. The data underlying the graphs can be found in S4 Data. (**G**) Scatter plot comparing gene scores for the screens under HL435 and DMSO treatment. Genes encoding components of the CRL4^{DCAF11} complex and the NEDD8-activating enzyme were highlighted. The data underlying this graph can be found in S4 Data. (**H**) Predicted structure of CRL4^{DCAF11} complex using Alphafold. Statistical significance was determined by one-way ANOVA. ****$P < 0.0001$.
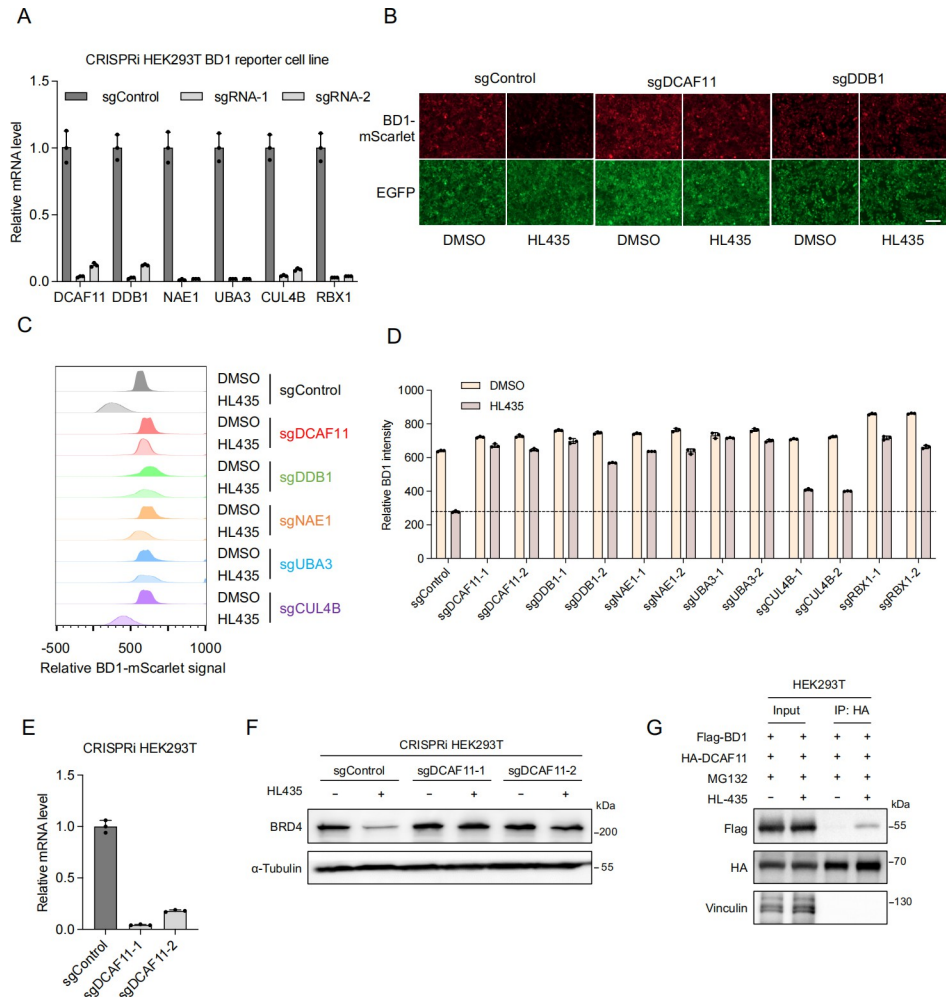
Fig 4. HL435 recruits CRL4^{DCAF11} complex to induce proteasomal degradation of BRD4. (**A**) Validation of knockdown efficiency of different hit genes in CRISPRi HEK293T reporter cells by RT-qPCR (mean ± SD, n = 3 technical replicates). (**B**) Representative fluorescent microscope fields for BD1 reporter levels in the reporter cells expressing sgRNAs targeting individual hit genes after DMSO or HL435 treatment (50 nM, 24 hours). Bar = 200 μm. (**C**) Relative BD1-mScarlet signal was quantified by flow cytometry for hit gene knockdown in BD1 reporter cells after DMSO or HL435 treatment (50 nM, 24 hours). (**D**) Quantification of the relative BD1 intensity in the indicated groups was shown in the bar graph (mean ± SD, n = 3 biological replicates). (**E**) Validation of knockdown efficiency of 2 sgRNAs targeting *DCAF11* in CRISPRi HEK293T reporter cells by RT-qPCR (mean ± SD, n = 3 technical replicates). (**F**) WB showing endogenous protein levels of BRD4 and α-tubulin in CRISPRi HEK293T cells expressing sgRNAs targeting *DCAF11* after DMSO or HL435 treatment (50 nM, 24 hours). (**G**) Co-immunoprecipitation analysis of HA-DCAF11 with Flag-BD1 in the absence or presence of HL435 (5 μM, 6 hours) in HEK293T cells. The data underlying the graphs in the figure can be found in S5 Data; the raw images for WB in the figure can be found in S1 Raw Images.

https://doi.org/10.1371/journal.pbio.3002550.g004

confirmed the requirement of DCAF11 in HL435-induced degradation of endogenous BRD4 (Fig 4E and 4F). Furthermore, we detected interaction between BRD4-BD1 and DCAF11 only in the presence of HL435, suggesting the formation of a ternary complex between BRD4, HL435, and DCAF11 (Fig 4G), which is the foundation for HL435-induced proteasomal degradation of BRD4. Taken together, these data indicate that the CRL4^{DCAF11} complex is responsible for HL435-induced proteasomal degradation of BRD4.

HL435 potently inhibits proliferation and induced apoptosis of tumor cells in vitro

BRD4 has been identified as a potential therapeutic target for tumors owing to its contribution to tumor pathogenesis [34,35]. As shown in Table 1, most of JQ1-alkenyl oxindole-conjugated compounds exhibited excellent antiproliferation abilities in breast cancer cell lines MCF-7 and MDA-MB-231, with HL435 performed the best overall. The antiproliferation activities of different compounds were positively correlated with their BRD4 degradation abilities, suggesting that BRD4 degradation contributed substantially to the antiproliferation activity of breast cancer. Notably, the half-maximal inhibitory concentrations (IC_{50}) of HL435 against 22RV1 (prostate cancer) was as low as 8.7 nM (Fig 5A), significantly superior to JQ1 (IC_{50} = 157 nM). To further explore the biological effects of HL435 on breast cancer, we performed flow cytometric analysis and WB to assess its influence on cell cycle and apoptosis in MCF-7 and MDA-MB-231 cells. HL435 acted similarly to JQ1 at low concentration, blocking the cell cycle at G0/G1 phase, while higher concentrations of HL435 arrested cell cycle at G2/M phase (Figs 5B, 5C, S6A and S6B). Consistent with the results of flow cytometric analysis, immunoblotting results showed that HL435 treatment up-regulated P53 and P21 levels and down-regulated the levels of cyclin D1 and cyclin B1 (Figs 5E and S6C), which contributed to block the G1/S and G2/M transitions. The ability of apoptosis induction by HL435 in breast cancer cells was >20-fold more potent than JQ1 (Figs 5D and S7A). Treatment with HL435 at 1.0 μM for 36 hours in MDA-MB-231 cells led to an apoptotic rate of 55.9 ± 1.9%, and the levels of cleaved caspase-9 and PARP1 were profoundly increased accordingly (Figs 5F and S7B). Oncogenes c-Myc is the key downstream protein used to evaluate the function of BRD4 [36]. As displayed in Figs 5E, S6C and S8A, both mRNA and protein levels of c-Myc were significantly down-regulated in breast cancer cells treated with HL435. These data indicated that HL435 not only exhibits excellent antiproliferative capacity against multiple tumor cell lines but also effectively arrests the cell cycle and induces apoptosis in breast cancer cells, validating the stronger therapeutic efficacy of degraders compared to inhibitors.

Table 1. Antiproliferation activities of compounds against breast cancer.

Compound	IC_{50} (μM)[a]		Compound	IC_{50} (μM)[a]	
	MCF-7	MDA-MB-231		MCF-7	MDA-MB-231
H1	116.80	2.17	H16	1.91	1.86
H2	147.40	36.54	H17	2.73	1.67
H3	6.66	1.96	H18	2.08	2.06
H4	21.24	1.37	H19	0.72	0.83
H5	2.66	1.58	H20	2.64	1.34
H6	0.49	0.48	H21	1.99	1.35
H7	0.46	0.31	H22	2.75	1.91
H8	0.77	0.81	H23	1.67	1.07
H9	0.87	0.81	H24	2.26	1.18
H10	0.95	0.82	H25	1.77	0.98
H11	0.19	0.50	H26	2.28	0.80
H12	3.39	1.89	H27(HL435)	0.38	0.21
H13	3.05	1.71	H28	4.02	1.45
H14	2.92	2.18	D27(HL389)	11.39	9.66
H15	1.37	2.04	JQ1	9.96	0.90

[a]IC_{50} values against cells proliferation were averages from triplicate measurements, determinated by CCK8 assay at 48 hours (JQ1 at 72 hours).

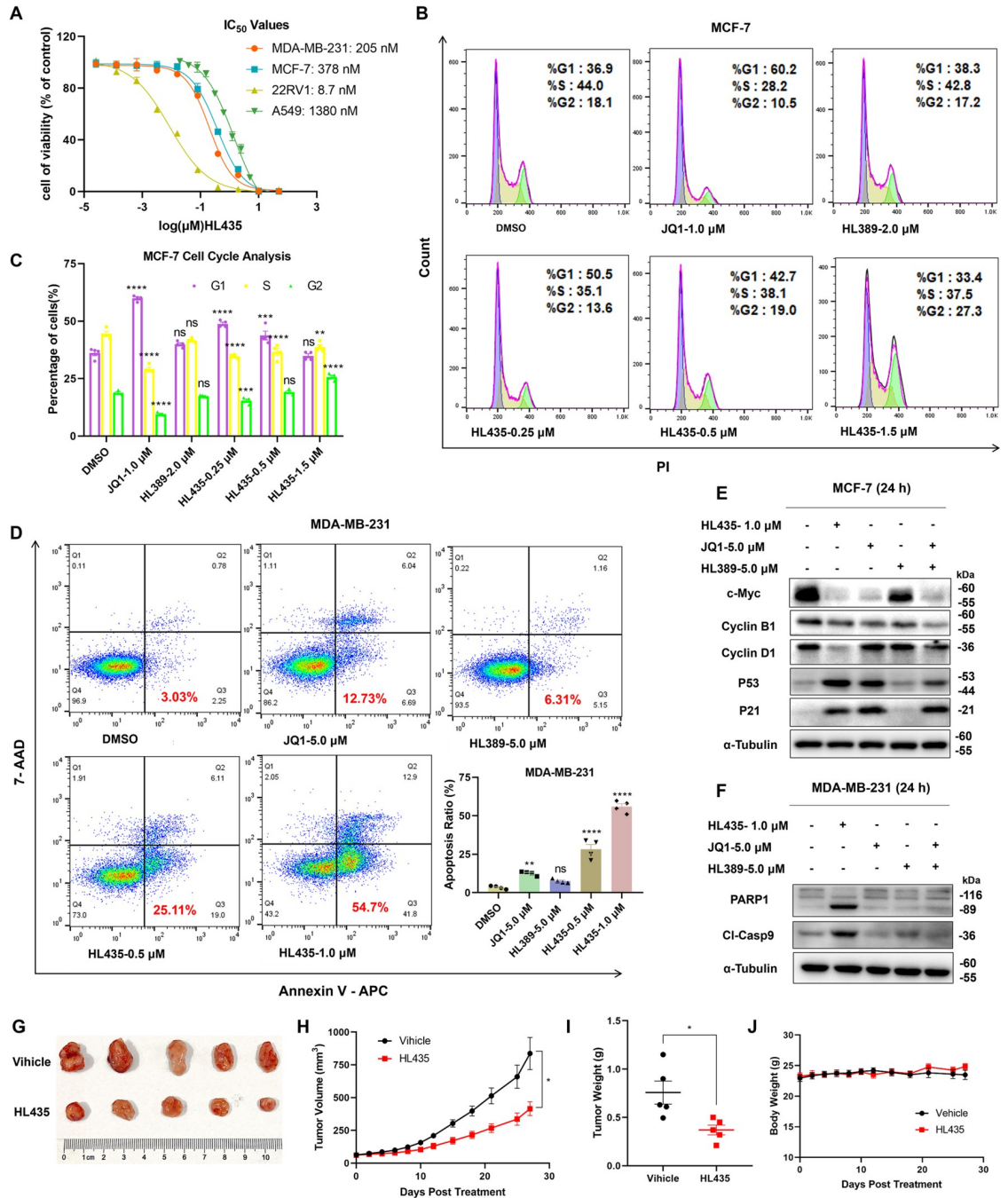https://doi.org/10.1371/journal.pbio.3002550.t001

Fig 5. HL435 exhibited excellent antitumor efficacy in vitro and in vivo. (**A**) IC$_{50}$ values of HL435 against multiple tumor cell lines, determinated by the CCK8 assay after 48-hour treatment. (**B**) Representative flow cytometry analysis results of the cell cycle in MCF-7 cells, treated with indicated compounds for 24 hours before stained with PI. (**C**) Quantitative statistical analysis of cell cycle for **B**. (**D**) Representative flow cytometry analysis results and quantitative statistical analysis of apoptosis; MDA-MB-231 cells were treated with indicated compounds for 36 hours before stained with a 7AAD/APC Apoptosis Detection kit. (**E**) Representative WB results of c-Myc and cycle relevant proteins in MCF-7 cells ($n = 3$). (**F**) Representative WB results of apoptosis relevant proteins in MDA-MB-231 cells ($n = 3$). (**G**) Picture of stripped xenograft tumors at the end of experiment (day 45). NOD-SICD mice bearing the MDA-MB-231 xenograft were daily administered with vehicle (10% DMSO + 90% corn oil, IP) or HL435 (20 mg/kg, IP) 6 days per week for 27 days. (**H**) Growth curve of xenograft tumors after treatment. (**I**) Weights of stripped xenograft tumors at day 45. (**J**) Body weight curves during treatment. The data underlying the graphs in the figure can be found in S5 Data; the raw images for WB in the figure can be found in S1 Raw Images. Data were presented as mean ± SEM ($n \geq 3$). One-way ANOVA or unpaired t test was employed to determine statistical significance. $^*p < 0.05$, $^{**}P < 0.01$, $^{***}P < 0.001$, $^{****}P < 0.0001$; ns, no statistical significance.

https://doi.org/10.1371/journal.pbio.3002550.g005

HL435 suppresses tumor growth in vivo

To evaluate the antitumor ability of HL435 in vivo, a mouse xenograft tumor model of MDA-MB-231 cells was employed. Mice bearing xenograft tumor were treated daily with HL435 (20 mg/kg) or vehicle (10% DMSO + 90% corn oil) 6 days per week. After 27 days of treatment, the HL435 treatment group attenuated tumor progression, with a tumor growth inhibition rate (TGI) of 54.34% (Fig 5H) and a 51.12% reduction in tumor weight (Fig 5I) compared to vehicle group. Meanwhile, the body weight of HL435-treated group was comparable to that of the vehicle group, and no obvious toxicity or adverse effects were observed throughout the experiment period (Fig 5J), indicating that HL435 was tolerated well. These data further validated the antitumor efficacy of HL435 in vivo, providing a promising drug-like lead compound for anticancer drug development.

Discussion and conclusions

Two alkenyl oxindoles (**10O5** and **AN1**) have been characterized as molecular glues that tether mHTT to LC3, enabling the lysosomal degradation of mHTT [32]. We initially sought to expand the versatility of this approach by conjugating alkenyl oxindoles to other substrate binding moieties, generating bifunctional molecules that may facilitate the degradation of various substrate proteins through the autophagy-lysosomal pathway. As a proof-of-principle, we generated a series of JQ1-alkenyl oxindole conjugates, from which we indeed identified molecules that potently degrade the target BRD4. However, when investigating the protein degradation mechanism of JQ1-alkenyl oxindole conjugates, we discovered that it does not occur via the autophagy-lysosomal pathway, but through the ubiquitin-proteasome system. We speculated that the alkenyl oxindole structure may recruit E3 ubiquitin ligase for their degradation activity. To determine the responsible E3 ubiquitin ligase, we conducted a pooled CRISPRi screening, from which we identified the $CRL4^{DCAF11}$ complex as a potential target for mediating the degradation activity of JQ1-alkenyl oxindole conjugates. We showed that alkenyl oxindoles can recruit DCAF11, thus acting as a novel PROTAC moiety for targeted protein degradation. Previously, the Cravatt [37] and Gray [38] groups, respectively, revealed that DCAF11 serves as an E3 ligase that can support protein degradation triggered by electrophilic PROTACs. Very recently, while we were preparing this manuscript for reviewing, similar findings were reported by Waldmann and Winter and colleagues [39]. Coincidentally but inevitably, their research work also validated that the degraders developed from conjugating with **10O5** recruit the E3 ubiquitin ligase $CRL4^{DCAF11}$ for the proteasomal degradation of substrate proteins, instead of autophagy-lysosome. As alkenyl oxindoles possesses Michael acceptor properties, they believed that they recruit DCAF11 through a covalent modification approach, potentially engaging with cysteine residues [39]. While a recent major report from the Ciulli and Winter labs identified a weak intrinsic affinity between BRD4 and DCAF11, and intramolecular glue degraders could enhance the surface complementarity between them by conformational modification, which can trigger productive ubiquitination and degradation of BRD4 [40]. These findings not only support our conclusions but also provide insights into the mechanism by which alkenyl oxindoles recruit DCAF11 to degrade target proteins.

Previous structure-activity studies on PROTACs have mainly focused on the effects of different linkers on degradation activity, with few studies on the structure-activity of the E3 ligase ligand part. In this study, we found that the ability to degrade BRD4 were significantly improved through structural optimization of E3 ligase ligands, and an excellent BRD4 degrader HL435 was identified, whose JQ1 moiety was conjugated with the trifluoromethyl-substituted alkenyl oxindole via PEG chain. The D_{max} of HL435 >99%, with DC_{50} values of 11.9 nM in MDA-MB-231 cells. To explore the druggability potential of heterobifunctional

compounds conjugated with alkenyl oxindoles, we evaluated their antitumor abilities both in vitro and in vivo. Most of heterobifunctional compounds exhibited more excellent antiproliferation abilities against breast cancer cells than JQ1 or alkenyl oxindoles, supporting the more excellent therapeutic potential of degraders compared to inhibitors. Consistent with the degradation efficiency of BRD4, HL435 showed the best antiproliferative activity overall, with an IC_{50} as low as 8.7 nM against prostate cancer cells 22RV1. In addition to outstanding antiproliferative abilities against multiple tumor cells, HL435 can effectively arrest the cell cycle and induce apoptosis in breast cancer cells by blocking BRD4 downstream signaling pathway in a concentration-dependent manner. Finally, the antitumor efficacy of HL435 in vivo was validated in a mouse MDA-MB-231 xenograft model, with good tolerability. These data suggested that HL435, a compound composed of structure modified alkenyl oxindole and BRD4 inhibitor JQ1, was a promising drug-like lead compound for anticancer drug development.

Although there are more than 600 E3 ubiquitin ligases in human cells, the ligand molecules currently available to recruit E3 ubiquitin ligases only cover less than 3% [18,19]. In addition, with the emergence of E3 ubiquitin ligase resistance, PROTACs based on the same E3 ubiquitin ligase ligand may be ineffective [41–43]. Therefore, the development of new E3 ubiquitin ligase ligands can not only solve the limitations of existing ligands, but also be a major way to expand the scope of PROTACs therapeutic targets and provide better treatment opportunities [26]. Moreover, as DCAF11 is localized in the nucleus, the identification of ligands capable of recruiting DCAF11 provides new possibilities for targeting the degradation of nuclear proteins.

In summary, we discovered alkenyl oxindole as a novel PROTAC moiety for targeted protein degradation via CRL4^{DCAF11} recruitment. We also developed JQ1-alkenyl oxindole-conjugated bifunctional molecules with high BRD4 degradation efficiencies in multiple cell lines and proved their anticancer effect both in vitro and in vivo. Our study expands the E3 toolbox available for PROTACs, which will potentially broaden the spectrum of degradable proteins and improve the efficiency of target degradation, as well as circumvent the acquired drug resistance caused by mutations in certain E3 ligases, providing new possibilities for drug discovery.

Materials and methods

Ethics statement

The animal experiment was conducted strictly according to animal ethics guidelines and the protocol (No. SYSU-IACUC-2023-000327), approved by the Institutional Animal Care and Use Committee (IACUC) of Sun Yat-sen University Cancer Center.

Cell lines culture and plasmid transfection

HCT116, MCF-7, 22RV1, A549, K562, THP-1, Hela, and HEK293T cell lines were previously obtained from ATCC and cryopreserved in our laboratory. MDA-MB-231 was newly purchased from Procell (Wuhan, China). *ATG4B*KO-Hela, *ATG5*KO-Hela, *ATG4B*KO-HCT116 were kindly gifts from Professor Li (Sun Yat-sen University). The CRISPRi HEK293T cell line was established by integrating dCas9-BFP-KRAB cassette into the CLYBL safe harbor locus via homology-directed repair (HDR) as described previously [33]. All cell lines were mycoplasma-free. HA-Ub and Flag-BRD4 plasmids were purchased from Miaoling Biology (Wuhan, China). Cell lines were cultured in RPMI-1640 medium (Gibco, Thermo Fisher Scientific, Waltham, MA, USA) or DMEM (Gibco) supplemented with 1% penicillin-streptomycin (Gibco) and 10% fetal bovine serum (FBS, sigma), the cultures were maintained in a CO_2 incubator at 37°C with 5% (v/v) CO_2. For transient transfection, HEK293T cells were seeded into 6-well plates and cultured to about 50% density, then cotransfected with HA-Ub and Flag-

BRD4 plasmids for 32 hours (Flag-BD1 and HA-DCAF11 plasmids for 48 hours) by Hieff Trans Liposomal Transfection Reagent (Yeasen, China).

DNA constructs

The coding sequence of BRD4 BD1 domain (amino acid N44-E168) was amplified from full-length of BRD4 cDNA in a pcDNA3.1-BRD4-3Flag with the forward primer (5′-ATGACGAT-GACAAGACTAGTaacccccccgcccccagagacctcca-3′) and reverse primer (5′-ccgccttcttctgtgggtag ctcatttatt-3′), and it was fused with mScarlet-P2A-EGFP from pRT117 vector into the pLVX-3Flag-Hygro vector with the forward primer (5′-ctacccacagaagaaGGCGGTGGCTCGGTGAG-CAA-3′) and reverse primer (5′-AGGGGCGGGATCCGCGGCCGCttactagtcggttcaactctaggtg-3′) by Hieff Clone Universal One Step Cloning Kit (YEASEN, 10922ES20). The coding sequence of DCAF11 (Youbio, L11006) was inserted into a pcDNA3.1-3HA vector with the forward primer (5′- TACCTGACTACGCTGGTACCatgggatcgcggaacagcagcag-3′) and reverse primer (5′- GATATCTGCAGAATTCctactggggtgaggaaaaggg-3′) by Hieff Clone Universal One Step Cloning Kit (YEASEN, 10922ES20).

CRISPRi screening

The overall CRIPSRi screening process was performed as described previously [33,44,45]. In brief, HEK293T cells harboring the BRD4 BD1 domain dual fluorescence reporter were infected with the sgRNA library targeting all human E1, E2, and E3 enzymes as described previously. The MOI value was controlled under 0.3 when library was transduced to the cells. The cells were selected by 2 μg/mL puromycin for 2 days. After expansion and puromycin selection, the cells were treated with DMSO and HL435, respectively. Five million cells were taken as "input" 24 hours later, and the remaining cells were subsequently collected for FACS, where the cells were sorted into the top 25% based on the ratio of mScarlet and EGFP signal. For each sample, cells corresponding to at least 4,000-fold over the library coverage were sorted per replicate. Sorted populations were collected and genomic DNA was isolated using DNAiso Reagent (Takara, 9770A). sgRNA cassettes were amplified by PCR and subjected to next-generation sequencing (NGS) by NovaSeq 6000 PE150. Sequencing results were analyzed using MAGeCK-iNC as previously described [33].

Cell viability assay

Cells were seeded in 96-well plates at a density of 2,000 to 4,000 cells per well. After overnight incubation, compounds were administered at the gradient concentrations for 2 to 3 days. Then, remove the old medium and add 100 μL fresh medium with 10% CCK8 reagent (Bimake; Selleck Chemicals; cat. no. B34304) for each well. And the plate was incubated in a cell incubator at 37˚C for 1 to 3 hours. The optical density (OD) value at 450 nm, which stands for the vitality of the cells, was detected with a BioTek Synergy H1 microplate reader. IC_{50} values of compounds against cell lines were calculated from triplicate measurements.

Co-immunoprecipitation and western blot analysis

Cells were lysed in RIPA buffer (Beyotime, Haimen, China) supplemented with phosphatase inhibitors (Bimake; Selleck Chemicals, Houston, TX, USA) or protease inhibitor cocktail (Roche, Basel, Switzerland). The protein in each sample was quantified by a BCA protein assay (Thermo Fisher, Rockford, IL) and boiled with 5×loading buffer (LB) for 5 minutes. For immunoprecipitation, 1 mg protein in each sample was incubated with anti-Flag (P2115, Beyotime, China) or anti-HA magnetic beads (P2121, Beyotime, China) overnight at 4˚C.

After washed away nonspecifically bound proteins, anti-Flag magnetic beads were boiled with 1× LB for transsexual washout. To separate protein samples, 8%, 10%, and 12% SDS-PAGE gels or 3% Tris-Acetate Polyacrylamide Gradient Gels were used and then transferred to a PVDF membrane (Millipore; Merck KGaA). About 5% skim milk was used to block membranes at room temperature (RT) for 1 hour. Primary antibodies were blotted at 4°C overnight. The next day, the membranes were slowly flipped in secondary antibodies conjugated with horseradish peroxidase for 1 hour at RT. Images were captured by Tanon 5200 (Shanghai, China). Image J was used to quantify the intensities of bands. The antibodies used in this paper were as below: Anti-α-Tubulin (T6047) , anti-LC3B (L7543) and anti-β-Actin were purchased from Sigma (St. Louis, MO, USA); Anti-BRD4 (13440), anti-PARP1 (9542), anti-Caspase 9 (9505), anti-HA (3724), and anti-Cyclin D1 (2922) were purchased from Cell Signaling Technology (Danvers, MA); Anti-Ubiquitin (sc-8017) was from Santa Cruz (Dallas, TX, USA). Anti-ATG4B (M134), anti-ATG5 (M153), and anti-Flag were from MBL (Tokyo, Japan); anti-Cyclin B1(55004-1-AP), anti-p53 (10442-1-AP), anti-p21 (10355-1-AP), anti-c-Myc (10828-1-AP), and anti-GAPDH (60004-1-Ig), anti-Vinculin (66305-1-Ig), goat anti-mouse IgG (H+L) (SA00001-1), and goat anti-rabbit IgG (H+L) (SA00001-2) were purchased from Proteintech.

Quantitative reverse transcription PCR (RT-qPCR)

MDA-MB-231 or MCF-7 cells were plated in 12-well plates and treated with compounds for 12 hours after overnight incubation. Total RNA was extracted using TRIzol (Invitrogen). A High-Capacity cDNA Reverse Transcription kit (Thermo Fisher Scientific) was used to create cDNA from purified RNA. The quantitative real-time PCR (qPCR) was conducted on a real-time fluorescence quantitative PCR equipment (light-Cycler480II, Roche) according to the protocol of SYBR Green qPCR Mix (Dongsheng Biotech, China). Results analyses were performed from 3 or 4 biological replicates; each data in biological replicate was triplicate. The expression level of genes was calculated with the $2^{-\Delta\Delta Ct}$ technique, and GAPDH or Tubulin was used as an internal reference. The expression level of each gene in the DMSO group was normalized to 1, and that of treatment groups were presented as fold-change relative to the DMSO group.

The primer sequences used were as follows:

GAPDH-F: GAGTCAACGGATTTGGTCGT, GAPDH-R: GACAAGCTTCCCGTTCTCAG;

BRD4-F: CTCCGCAGACATGCTAGTGA, BRD4-R: GTAGGATGACTGGGCCTCTG;

c-MYC-F: CACCGAGTCGTAGTCGAGGT, c-MYC-R: GCTGCTTAGACGCTGGATTT;

P21-F: TGTCCGTCAGAACCCATGC, P21-R: AAAGTCGAAGTTCCATCGCTC;

DCAF11-F: CAATGATCTGGGCTTCACTGAT, DCAF11-R: TCTTGGCAAGCAGACATGAAT;

DDB1-F: ATGTCGTACAACTACGTGGTAAC, DDB1-R: CGAAGTAAAGTGTCCGGTCAC;

NAE1-F: ACCTGTTCGAGGCACAATTCC, NAE1-R: TCTTTGCTTTTTCACGGTAAACG;

UBA3-F: CGATCTGGACCCTTCACACAC, UBA3-R: GCCAGCTCCAATGACTAGAAC;

CUL4B-F: ACTCCTCCTTTACAACCCAGG, CUL4B-R: TCTTCGCATCAAACCCTACAAAC;

RBX1-F: TTGTGGTTGATAACTGTGCCAT, RBX1-R: GACGCCTGGTTAGCTTGACAT;

Tubulin-F: ACCTTAACCGCCTTATTAGCCA, Tubulin-R: ACATTCAGGGCTCCATCAAATC.

Cell cycle assay

The influence of compounds on the cell cycle was detected by cell flow cytometry following instructions of the Cell Cycle Analysis Kit (C1052, Beyotime). In brief, seed cells into a 6-well plate at an appropriate density. After overnight incubation, compounds were administered at the respective concentration for 24 hours. Precooled PBS was used to wash cells before and after centrifugation, followed by overnight fixation in 70% ethanol at 4˚C. On the next day, ethanol was removed by centrifugation, then cells were dealt with RNase for 30 minutes at 37˚C. Subsequently, they were stained with propidium iodide (PI) at RT for an additional 30 minutes. If stored at 4˚C, the stained cells can be detected on a flow cytometer (BD FACSCalibur, BD Biosciences, USA) within 24 hours and analyzed for cell cycle distribution using FlowJo software.

Cell apoptosis assay

The effect of compounds on inducing apoptosis was detected using cell flow cytometry according to the instructions of Annexin V APC/7-AAD apoptosis kit (AP105-100, liankebio, China). In brief, seed cells into a 6-well plate at an appropriate density. On the next day, compounds were administered at the respective concentrations for 36 hours. Around 500 μL 1× binding buffer was used to resuspend the harvested cells, and then add Annexin V-APC (5 μL) and 7-AAD (10 μL). Gently mix the solution and incubate it in the dark at RT for 5 minutes. Finally, a flow cytometer (BD FACSCalibur, BD Biosciences, USA) was employed to detect the cells as soon as possible.

Animal experiment

Animal experiment was performed at the Experimental Animal Center of Sun Yat-sen University (East Campus), and female NOD-SCID mice were purchased from Guangdong Yaokang Biotechnology. Inject subcutaneously 5 million MDA-MB-231 cells on the right dorsal side of each mouse at the age of 6 to 7 weeks. When tumors size reached 60 to 70 mm^3 about half a month later, mice were randomly divided into 2 groups. Mice were daily injected with vehicle (10% DMSO + 90% corn oil, IP) or HL435 (20 mg/kg, IP) 6 days per week for 27 days. Volume of xenograft tumor and body weight of each mouse were measured every 2 to 4 days. Volume of xenograft tumor = length × width^2/2. Kill all of mice at day 27 posttreatment and xenograft tumors were excised for weight measurement. TGI (%) = [1 − ($TV_{Treatment/Dx}$ − $TV_{Treatment/D1}$) / ($TV_{Vehicle/Dx}$ − $TV_{Vehicle/D1}$)] × 100%, X = days posttreament.

Chemistry

Unless otherwise stated, all solvents and the compounds without provided synthesis routes were commercially purchased. All solvents were purified and dried according to standard methods before use. The spectra of ^{1}H nuclear magnetic resonance (NMR) was recorded on a Varian instrument (500 MHz or 400 MHz), and the tetramethylsilane signal or residual protio solvent signals was used as the internal standard. ^{13}C NMR was recorded on a Varian instrument (125 MHz or 100 MHz). Data for ^{1}H NMR were recorded as follows: chemical shift (δ, ppm), multiplicity (s = singlet, d = doublet, t = triplet, m = multiplet, q = quartet or unresolved, coupling constant (s) in Hz, integration). Data for ^{13}C NMR were reported in terms of chemical shift (δ, ppm). The progress of the reaction was monitored by thin-layer

chromatography (TLC) on glass plates coated with a fluorescent indicator (GF254). Flash column chromatography was performed on silica gel (200 to 300 mesh). The ESI ionization sources were employed to obtain high-resolution mass spectra (HRMS). The purity of final key products was confirmed by a Waters e2695 HPLC system equipped with an XBridge C18 (5 um, 4.6 × 250 mm) and eluted with methanol/water (97.5:2.5) at a flow rate of 1.0 mL/minute. The yields indicated were from single step reactions. All compounds used in biological tests have been further purified by preparative liquid chromatography, and all of them showed >95% purity using the HPLC methods described above.

Supporting information

S1 Fig. All compounds we developed could degrade BRD4 in a concentration-dependent manner. Western blotting results for BRD4 degradation. Image J was employed for relative quantitative analysis. The raw images for WB in the figure can be found in S1 Raw Images. (TIF)

S2 Fig. BRD4 degradation activity between different configurations of H6. The raw images for WB in the figure can be found in S1 Raw Images. (TIF)

S3 Fig. HL435 degraded BRD4 in concentration- and time-dependent manner in MCF-7 cells. (**A**) Representative WB results for concentration-dependent studies of BRD4 degradation. (**B**) Representative WB results for kinetics studies of BRD4 degradation. Image J was employed for relative quantitative analysis. The raw images for WB in the figure can be found in S1 Raw Images. (TIF)

S4 Fig. HL435 potently degraded BRD4 in multiple cell lines. WB results for BRD4 degradation. Image J was employed for relative quantitative analysis. The raw images for WB in the figure can be found in S1 Raw Images. (TIF)

S5 Fig. Compounds conjugated alkenyl oxindoles degraded BRD4 via ubiquitin-proteasome system. (**A**) Structure of compounds conjugated alkenyl oxindoles. (**B**) Autophagy-lysosome inhibitor CQ or Baf cannot rescue the degradation of BRD4 by **H1**. (**C**) **H1** degraded BRD4 independent of LC3 and autophagosomes. (**D**) Proteasome inhibitor MG132 but not autophagy inhibitor CQ or Baf could rescue the degradation of BRD4 by **H6** or **H7**. Cells were pretreated with MG132, CQ, or Baf for 2 hours, followed by **H6** or **H7** treatment for 6 hours. (**E**) Inhibitors of the ubiquitin-protease system could rescue the degradation of BRD4 by **H6**. Cells were pretreated with PYR-41 or MG132 for 2 hours, followed by **H6** treatment for 6 hours. The raw images for WB in the figure can be found in S1 Raw Images. (TIF)

S6 Fig. HL435 arrested cell cycle in MDA-MB-231 cells. (**A**) Representative flow cytometry analysis results of the cell cycle. MDA-MB-231 cells were treated with indicated compounds for 24 hours before stained with PI. (**B**) Quantitative statistical analysis of cell cycle for **A**. (**C**) Representative WB results of cycle relevant proteins in MDA-MB-231 cells. The data underlying the graphs in the figure can be found in S5 Data; the raw images for WB in the figure can be found in S1 Raw Images. Data were presented as mean ± SEM (n = 3). Statistical significance was determined by one-way ANOVA. $^{**}P < 0.01$, $^{***}P < 0.001$, $^{****}P < 0.0001$; ns, no statistical significance. (TIF)

S7 Fig. HL435 induced cell apoptosis in MCF-7 cells. (**A**) Representative flow cytometry analysis results and quantitative statistical analysis of apoptosis; MCF-7 cells were treated with indicated compounds for 36 hours before stained with an 7AAD/APC Apoptosis Detection kit. (**B**) Representative WB results of apoptosis-relevant proteins. The data underlying the graphs in the figure can be found in S5 Data; the raw images for WB in the figure can be found in S1 Raw Images. Data were presented as mean ± SEM (n = 3). Statistical significance was determined by one-way ANOVA. ***$P < 0.001$, ****$P < 0.0001$; ns, no statistical significance. (TIF)

S8 Fig. Effects of HL435 on the transcript levels of *c-MYC* (A) and *P21* (B) in breast cancer cell lines. Cells were treated with indicated compounds for 12 hours; GAPDH was used as internal reference. The data underlying the graphs in the figure can be found in S5 Data. Data were presented as mean ± SEM. Statistical significance was determined by one-way ANOVA. *$P < 0.05$, ***$P < 0.001$, ****$P < 0.0001$; ns, no statistical significance. (TIF)

S1 Data. The synthetic methods of compounds H1-H28. (PDF)

S2 Data. ^{1}H and ^{13}C NMR Spectra of compounds H1-H28 and D27. (PDF)

S3 Data. The HPLC data for different configurations of H6 under different preservation conditions. (PDF)

S4 Data. CRISPRi screening results and sgRNA sequence of CRL4^{DCAF11} complex. (XLSX)

S5 Data. Underlying numerical data for Figs 2C, 2E, 2F, 2H, 2K, 2O, 3D, 4A, 4D, 4E, 5A, 5C, 5D, 5H, 5I, 5J, S6B, S7A and S8. (XLSX)

S1 Raw Images. Raw images for all WB. (PDF)

Acknowledgments

Author Contributions

Conceptualization: Liang Hong, Rui Wang, Guofeng Li.

Data curation: Ying Wang, Man Zhao, Aima Huang, Fan Sun, Lu Chen, Risheng Lin, Ming Zhang, Shiyu Xu, Zhihui Sun, Liang Hong, Rui Wang, Ruilin Tian, Guofeng Li.

Formal analysis: Ying Wang, Liang Hong, Rui Wang, Ruilin Tian.

Funding acquisition: Tianzi Wei, Ming Zhang, Liang Hong, Rui Wang, Ruilin Tian.

Investigation: Ying Wang, Tianzi Wei, Man Zhao, Rui Wang, Guofeng Li.

Methodology: Ying Wang, Tianzi Wei, Man Zhao, Aima Huang, Fan Sun, Lu Chen, Risheng Lin, Yubao Xie, Ming Zhang.

Project administration: Ying Wang, Tianzi Wei, Man Zhao, Aima Huang, Fan Sun, Lu Chen, Risheng Lin, Yubao Xie, Ming Zhang, Shiyu Xu, Zhihui Sun.

Resources: Ming Zhang, Liang Hong, Rui Wang, Ruilin Tian, Guofeng Li.

Software: Ying Wang, Liang Hong, Rui Wang, Ruilin Tian.

Supervision: Ying Wang, Tianzi Wei, Ming Zhang, Liang Hong, Rui Wang, Ruilin Tian, Guofeng Li.

Validation: Ying Wang, Tianzi Wei, Fan Sun, Lu Chen, Ming Zhang, Ruilin Tian.

Visualization: Ying Wang, Tianzi Wei, Man Zhao, Aima Huang, Fan Sun, Lu Chen, Risheng Lin, Yubao Xie, Ming Zhang, Shiyu Xu, Zhihui Sun.

Writing – original draft: Ying Wang, Tianzi Wei, Man Zhao.

Writing – review & editing: Ying Wang, Tianzi Wei, Man Zhao, Liang Hong, Rui Wang, Ruilin Tian, Guofeng Li.

References

1. Deshaies RJ. Multispecific drugs herald a new era of biopharmaceutical innovation. Nature. 2020; 580 (7803):329–338. https://doi.org/10.1038/s41586-020-2168-1 PMID: 32296187

2. Winter GE, Buckley DL, Paulk J, Roberts JM, Souza A, Dhe-Paganon S, et al. Phthalimide conjugation as a strategy for *in vivo* target protein degradation. Science. 2015; 348(6241):1376–1381.

3. Wu T, Yoon H, Xiong Y, Dixon-Clarke SE, Nowak RP, Fischer ES. Targeted protein degradation as a powerful research tool in basic biology and drug target discovery. Nat Struct Mol Biol. 2020; 27(7):605– 614. https://doi.org/10.1038/s41594-020-0438-0 PMID: 32541897

4. Salami J, Crews CM. Waste disposal—An attractive strategy for cancer therapy. Science. 2017; 355 (6330):1163–1167. https://doi.org/10.1126/science.aam7340 PMID: 28302825

5. Ciechanover A. Intracellular Protein Degradation: From a Vague Idea, through the Lysosome and the Ubiquitin–Proteasome System, and onto Human Diseases and Drug Targeting. Angew Chem Int Ed. 2005; 44(37):5944–5967.

6. Dikic I. Proteasomal and Autophagic Degradation Systems. Annu Rev Biochem. 2017; 86(1):193–224.

7. Lu K, den Brave F, Jentsch S. Pathway choice between proteasomal and autophagic degradation. Autophagy. 2017; 13(10):1799–1800. https://doi.org/10.1080/15548627.2017.1358851 PMID: 28813181

8. Nalawansha DA, Crews CM. PROTACs: An Emerging Therapeutic Modality in Precision Medicine. Cell Chem Bio. 2020; 27(8):998–1014. https://doi.org/10.1016/j.chembiol.2020.07.020 PMID: 32795419

9. Ding Y, Fei Y, Lu B. Emerging New Concepts of Degrader Technologies. Trends Pharmacol Sci. 2020; 41(7):464–474. https://doi.org/10.1016/j.tips.2020.04.005 PMID: 32416934

10. Takahashi D, Moriyama J, Nakamura T, Miki E, Takahashi E, Sato A, et al. AUTACs: Cargo-Specific Degraders Using Selective Autophagy. Mol Cell. 2019; 76(5):797–810.e710. https://doi.org/10.1016/j.molcel.2019.09.009 PMID: 31606272

11. Banik SM, Pedram K, Wisnovsky S, Ahn G, Riley NM, Bertozzi CR. Lysosome-targeting chimaeras for degradation of extracellular proteins. Nature. 2020; 584(7820):291–297. https://doi.org/10.1038/s41586-020-2545-9 PMID: 32728216

12. Cao C, He M, Wang L, He Y, Rao Y. Chemistries of bifunctional PROTAC degraders. Chem Soc Rev. 2022; 51(16):7066–7114. https://doi.org/10.1039/d2cs00220e PMID: 35916511

13. Mullard A. Targeted protein degraders crowd into the clinic. Nat Rev Drug Discov. 2021; 20(4):247– 250. https://doi.org/10.1038/d41573-021-00052-4 PMID: 33737725

14. Li J, Chen X, Lu A, Liang C. Targeted protein degradation in cancers: Orthodox PROTACs and beyond. Innovation. 2023; 4(3):100413. https://doi.org/10.1016/j.xinn.2023.100413 PMID: 37033156

15. Kong NR, Jones LH. Clinical Translation of Targeted Protein Degraders. Clin Pharmacol Ther. 2023; 114(3):558–568. https://doi.org/10.1002/cpt.2985 PMID: 37399310

16. Mullard A. First targeted protein degrader hits the clinic. Nat Rev Drug Discov. 2019; 18(4):237–239. https://doi.org/10.1038/d41573-019-00043-6 PMID: 30936511

17. Burslem GM, Crews CM. Proteolysis-Targeting Chimeras as Therapeutics and Tools for Biological Discovery. Cell. 2020; 181(1):102–114. https://doi.org/10.1016/j.cell.2019.11.031 PMID: 31955850

18. Clague MJ, Heride C, Urbé S. The demographics of the ubiquitin system. Trends Cell Biol. 2015; 25 (7):417–426. https://doi.org/10.1016/j.tcb.2015.03.002 PMID: 25906909

19. Mi D, Li Y, Gu H, Li Y, Chen Y. Current advances of small molecule E3 ligands for proteolysis-targeting chimeras design. Eur J Med Chem. 2023; 256:115444. https://doi.org/10.1016/j.ejmech.2023.115444 PMID: 37178483

20. Wei J, Meng F, Park K-S, Yim H, Velez J, Kumar P, et al. Harnessing the E3 Ligase KEAP1 for Targeted Protein Degradation. J Am Chem Soc. 2021; 143(37):15073–15083. https://doi.org/10.1021/jacs.1c04841 PMID: 34520194

21. Du G, Jiang J, Henning NJ, Safaee N, Koide E, Nowak RP, et al. Exploring the target scope of KEAP1 E3 ligase-based PROTACs. Cell Chem Bio. 2022; 29(10):1470–1481.e31. https://doi.org/10.1016/j.chembiol.2022.08.003 PMID: 36070758

22. Tong B, Spradlin JN, Novaes LFT, Zhang E, Hu X, Moeller M, et al. A Nimbolide-Based Kinase Degrader Preferentially Degrades Oncogenic BCR-ABL. ACS Chem Biol. 2020; 15(7):1788–1794. https://doi.org/10.1021/acschembio.0c00348 PMID: 32568522

23. Luo M, Spradlin JN, Boike L, Tong B, Brittain SM, McKenna JM, et al. Chemoproteomics-enabled discovery of covalent RNF114-based degraders that mimic natural product function. Cell Chem Bio. 2021; 28(4):559–566.e15. https://doi.org/10.1016/j.chembiol.2021.01.005 PMID: 33513350

24. Li L, Mi D, Pei H, Duan Q, Wang X, Zhou W, et al. In vivo target protein degradation induced by PROTACs based on E3 ligase DCAF15. Signal Transduct Target Ther. 2020; 5(1):129. https://doi.org/10.1038/s41392-020-00245-0 PMID: 32713946

25. Zhang X, Crowley VM, Wucherpfennig TG, Dix MM, Cravatt BF. Electrophilic PROTACs that degrade nuclear proteins by engaging DCAF16. Nat Chem Biol. 2019; 15(7):737–746. https://doi.org/10.1038/s41589-019-0279-5 PMID: 31209349

26. Békés M, Langley DR, Crews CM. PROTAC targeted protein degraders: the past is prologue. Nat Rev Drug Discov. 2022; 21(3):181–200. https://doi.org/10.1038/s41573-021-00371-6 PMID: 35042991

27. Lee J, Lee Y, Jung YM, Park JH, Yoo HS, Park J. Discovery of E3 Ligase Ligands for Target Protein Degradation. Molecules. 2022; 27(19). https://doi.org/10.3390/molecules27196515 PMID: 36235052

28. Chaudhari P, Bari S, Surana S, Shirkhedkar A, Wakode S, Shelar S, et al. Logical synthetic strategies and structure-activity relationship of indolin-2-one hybrids as small molecule anticancer agents: An overview. J Mol Struct. 2022; 1247:131280.

29. Andreani A, Granaiola M, Locatelli A, Morigi R, Rambaldi M, Varoli L, et al. Cytotoxic activities of substituted 3-(3,4,5-trimethoxybenzylidene)-1,3-dihydroindol-2-ones and studies on their mechanisms of action. Eur J Med Chem. 2013; 64:603–612. https://doi.org/10.1016/j.ejmech.2013.03.033 PMID: 23685944

30. Hopkins TG, Marples M, Stark D. Sunitinib in the management of gastrointestinal stromal tumours (GISTs). Eur J Surg Oncol. 2008; 34(8):844–850. https://doi.org/10.1016/j.ejso.2007.10.011 PMID: 18082353

31. Yousefian M, Ghodsi R. Structure–activity relationship studies of indolin-2-one derivatives as vascular endothelial growth factor receptor inhibitors and anticancer agents. Arch Pharm. 2020; 353 (12):2000022. https://doi.org/10.1002/ardp.202000022 PMID: 32885522

32. Li Z, Wang C, Wang Z, Zhu C, Li J, Sha T, et al. Allele-selective lowering of mutant HTT protein by HTT–LC3 linker compounds. Nature. 2019; 575(7781):203–209. https://doi.org/10.1038/s41586-019-1722-1 PMID: 31666698

33. Tian R, Gachechiladze MA, Ludwig CH, Laurie MT, Hong JY, Nathaniel D, et al. CRISPR Interference-Based Platform for Multimodal Genetic Screens in Human iPSC-Derived Neurons. Neuron. 2019; 104 (2):239–255e12. https://doi.org/10.1016/j.neuron.2019.07.014 PMID: 31422865

34. Duan Y, Guan Y, Qin W, Zhai X, Yu B, Liu H. Targeting Brd4 for cancer therapy: inhibitors and degraders. Med Chem Commun. 2018; 9(11):1779–1802. https://doi.org/10.1039/c8md00198g PMID: 30542529

35. Stathis A, Bertoni F. BET Proteins as Targets for Anticancer Treatment. Cancer Discov. 2018; 8(1):24–36. https://doi.org/10.1158/2159-8290.CD-17-0605 PMID: 29263030

36. Lovén J, Hoke Heather A, Lin Charles Y, Lau A, Orlando David A, Vakoc Christopher R, et al. Selective Inhibition of Tumor Oncogenes by Disruption of Super-Enhancers. Cell. 2013; 153(2):320–334. https://doi.org/10.1016/j.cell.2013.03.036 PMID: 23582323

37. Zhang X, Luukkonen LM, Eissler CL, Crowley VM, Yamashita Y, Schafroth MA, et al. DCAF11 Supports Targeted Protein Degradation by Electrophilic Proteolysis-Targeting Chimeras. J Am Chem Soc. 2021; 143(13):5141–5149. https://doi.org/10.1021/jacs.1c00990 PMID: 33783207

38. Sarott RC, You I, Li Y-D, Toenjes ST, Donovan KA, Seo P, et al. Chemical Specification of E3 Ubiquitin Ligase Engagement by Cysteine-Reactive Chemistry. J Am Chem Soc. 2023; 145(40):21937–21944. https://doi.org/10.1021/jacs.3c06622 PMID: 37767920

39. Xue G, Xie J, Hinterndorfer M, Cigler M, Dötsch L, Imrichova H, et al. Discovery of a Drug-like, Natural Product-Inspired DCAF11 Ligand Chemotype. Nat Commun. 2023; 14(1):7908. https://doi.org/10.1038/s41467-023-43657-6 PMID: 38036533

40. Hsia O, Hinterndorfer M, Cowan AD, Iso K, Ishida T, Sundaramoorthy R, et al. Targeted protein degradation via intramolecular bivalent glues. Nature. 2024; 627(8002):204–211. https://doi.org/10.1038/s41586-024-07089-6 PMID: 38383787

41. Gooding S, Ansari-Pour N, Towfic F, Ortiz Estévez M, Chamberlain PP, Tsai K-T, et al. Multiple cereblon genetic changes are associated with acquired resistance to lenalidomide or pomalidomide in multiple myeloma. Blood. 2021; 137(2):232–237. https://doi.org/10.1182/blood.2020007081 PMID: 33443552

42. Shirasaki R, Matthews GM, Gandolfi S, de Matos SR, Buckley DL, Raja Vora J, et al. Functional Genomics Identify Distinct and Overlapping Genes Mediating Resistance to Different Classes of Heterobifunctional Degraders of Oncoproteins. Cell Rep. 2021; 34(1):108532. https://doi.org/10.1016/j.celrep.2020.108532 PMID: 33406420

43. Zhang L, Riley-Gillis B, Vijay P, Shen Y. Acquired Resistance to BET-PROTACs (Proteolysis-Targeting Chimeras) Caused by Genomic Alterations in Core Components of E3 Ligase Complexes. Mol Cancer Ther. 2019; 18 (7):1302–1311. https://doi.org/10.1158/1535-7163.MCT-18-1129 PMID: 31064868

44. Tian R, Abarientos A, Hong J, Hashemi SH, Yan R, Drager N, et al. Genome-wide CRISPRi/a screens in human neurons link lysosomal failure to ferroptosis. Nat Neurosci. 2021; 24(7):1020–1034. https://doi.org/10.1038/s41593-021-00862-0 PMID: 34031600

45. Samelson AJ, Tran QD, Robinot R, Carrau L, Rezelj VV, Kain AM, et al. BRD2 inhibition blocks SARS-CoV-2 infection by reducing transcription of the host cell receptor ACE2. Nat Cell Biol. 2022; 24(1):24–34. https://doi.org/10.1038/s41556-021-00821-8 PMID: 35027731